

***In vivo* imaging of orthotopic prostate cancer with far-red gene reporter fluorescence tomography and *in vivo* and *ex vivo* validation**

Yujie Lu
Chinmay D. Darne
I-Chih Tan
Grace Wu
Nathaniel Wilganowski
Holly Robinson
Ali Azhdarinia
Banghe Zhu
John C. Rasmussen
Eva M. Sevick-Muraca

In vivo imaging of orthotopic prostate cancer with far-red gene reporter fluorescence tomography and *in vivo* and *ex vivo* validation

Yujie Lu, Chinmay D. Darne, I-Chih Tan, Grace Wu, Nathaniel Wilganowski, Holly Robinson, Ali Azhdarinia, Banghe Zhu, John C. Rasmussen, and Eva M. Sevick-Muraca

University of Texas Health Science Center at Houston, The Brown Foundation Institute of Molecular Medicine, Center for Molecular Imaging, 1825 Pressler Street SRB 330, Houston, Texas 77030

Abstract. Fluorescence gene reporters have recently become available for excitation at far-red wavelengths, enabling opportunities for small animal *in vivo* gene reporter fluorescence tomography (GRFT). We employed multiple projections of the far-red fluorescence gene reporters IFP1.4 and iRFP, excited by a point source in transillumination geometry in order to reconstruct the location of orthotopically implanted human prostate cancer (PC3), which stably expresses the reporter. Reconstruction was performed using a linear radiative-transfer-based regularization-free tomographic method. Positron emission tomography (PET) imaging of a radiolabeled antibody-based agent that targeted epithelial cell adhesion molecule overexpressed on PC3 cells was used to confirm *in vivo* GRFT results. Validation of GRFT results was also conducted from *ex vivo* fluorescence imaging of resected prostate tumor. In addition, in mice with large primary prostate tumors, a combination of GRFT and PET showed that the radiolabeled antibody did not penetrate the tumor, consistent with known tumor transport limitations of large (~150 kDa) molecules. These results represent the first tomography of a living animal using far-red gene reporters.

© 2013 Society of Photo-Optical Instrumentation Engineers (SPIE) [DOI: [10.1117/1.JBO.18.10.101305](https://doi.org/10.1117/1.JBO.18.10.101305)]

Keywords: gene reporter fluorescence tomography; reconstruction algorithm; imaging system; imaging validation; fluorescence gene reporter.

Paper 130075SSRR received Feb. 12, 2013; revised manuscript received May 21, 2013; accepted for publication May 21, 2013; published online Jun. 25, 2013.

1 Introduction

Due to the absence of background signal and facile operation, small animal bioluminescence imaging of well-known luciferase gene reporter systems has significantly advanced studies.¹ However, both bioluminescence and fluorescence gene reporter imaging (referred to here as BGRI and FGRI, respectively) suffer from strong light attenuation since most gene reporters emit light in the visible wavelength region where tissue absorbance is high.² In addition, strong tissue autofluorescence results from excitation at visible light wavelengths, further compromising the performance of FGRI. Upon using excitation light at far-red or near-infrared (NIR) wavelengths, tissue absorption and autofluorescence are significantly reduced, enabling fluorescence gene reporters that can be excited at these wavelengths ideal for FGRI. However, the limited availability of far-red and NIR fluorescence gene reporters has restricted the development of FGRI. Recently, Roger Tsien and coworkers³ developed a far-red fluorescence gene reporter, IFP1.4, which could be excited by a red laser diode emitting at 690 nm for collection of 710 to 720 nm fluorescent photons. The protein was created through structure-based engineering of a bacteriophytochrome that fluoresces when it associates with ubiquitous biliverdin, the catabolic by-product of hemoglobin metabolism. More recently, Filonov et al.⁴ developed an analog of IFP1.4, iRFP,

with greater fluorescent yield that further enhances the opportunity for gene reporter fluorescence tomography (GRFT).

Fluorescence tomography makes use of the surface measurement of emitted light for mathematical reconstruction of the source of light emission.⁵ Compared to bioluminescence tomography, GRFT could potentially result in more facile and robust three-dimensional (3-D) image reconstructions due to a higher photon count rate and the ability to conduct time-dependent measurements, as well as the possible combinations of multiple incident excitation patterns with multiple projection measurements of emitted light. However, acquisition of multiple projections requires multiple excitation sources/detectors,⁶ a conical mirror assembly,⁷ or a rotating gantry-based imaging system, the latter of which could also benefit with the integration of other imaging modalities, such as nuclear [positron emission tomography (PET), single-photon emission computed tomography (SPECT)] and x-ray computed tomography (CT).

Herein, we present the first tomographic small animal reconstructions of far-red fluorescence gene reporters in an orthotopic prostate cancer tumor model stably expressing IFP1.4 or iRFP. The methods employed a trimodal (fluorescence/ μ PET/ μ CT) gantry-based imaging system and a linear, regularization-free reconstruction algorithm employing the third-order simplified harmonics spherical approximation (SP₃) to the radiative transfer equation (RTE) and *a priori* anatomical information obtained from μ CT. With IFP1.4 and iRFP stable expression in orthotopically implanted human tumor cells, the tomographic results demonstrate that far-red GRFT can provide good 3-D reconstruction for deeply located primary tumors as validated

Address all correspondence to: Eva M. Sevick-Muraca and Yujie Lu, University of Texas Health Science Center at Houston, The Brown Foundation Institute of Molecular Medicine, Center for Molecular Imaging, 1825 Pressler Street SRB 330, Houston, Texas 77030. E-mail: Eva.Sevick@uth.tmc.edu; Yujie.Lu@uth.tmc.edu

in vivo using an exogenous PET agent as well *ex vivo* fluorescence imaging.

2 Materials and Methods

Human prostate cancer (PC3) cells were transfected by the IFP1.4 or iRFP reporter genes for our experiments. For IFP1.4 gene reporter, a mammalian viral vector was used to transfect cells and high expressing cells were selected and sorted on the basis of 710 nm fluorescence. Transfection with the plasmid was not efficient as it was for the iRFP gene reporter. For iRFP gene reporter, piRFP plasmid (Addgene, Cambridge, MA) was used to deliver iRFP reporter gene into the cells by using the electroporation method. Transfected cells were grown under G418 selection in Dulbecco's modified eagle medium-F12/10% fetal bovine serum growing medium and were sorted depending on 710 nm fluorescence intensity. Male nu/nu mice (6 to 8 weeks old; Charles River Laboratories, Wilmington, MA) were prepared for the experiments. The transfected PC3 cells (10^6 cells) were orthotopically implanted in the dorsal prostate of each mouse. Planar fluorescence imaging was used to longitudinally monitor tumor growth every week and animals were fed an alfalfa-free food to reduce autofluorescence for imaging^{8,9} and tomography measurements. Animal studies were approved by the Animal Welfare Committee at the University of Texas Health Science Center at Houston and the Association for Assessment and Accreditation of Laboratory Animal Care.

The trimodal (fluorescence/ μ PET/ μ CT) imaging system was developed using a commercial, Siemens Inveon scanner as previously described,¹⁰ but modified to enable far-red GRFT. Briefly, the SPECT component of the commercial imaging system was replaced with a miniaturized Gen III intensified charge-coupled device (ICCD) and an illumination system within the CT gantry. For this work, the illumination system consisted of a 690-nm laser diode (Intense Inc., North Brunswick, NJ), laser mount, diode driver, temperature controller (Thorlabs, TCDLM9, LDC205, TED200, Newton, NJ), and two scannable mirrors. A 690-nm bandpass filter (Semrock Inc., Rochester, NY) was used to insure the monochromatic light and the collected light were passed through the 720-nm filters (Semrock Inc.) before being incident on the photocathode stage of the image intensifier.^{8,9} Although the fluorescence imaging system is capable of time-dependent measurements through gain modulation of the laser diode and photocathode, herein we conducted time-independent, continuous wave measurements since we expected limitations in the number of fluorescent photons counted. With the gantry-based system design, acquisition of multiple projection images were made by transilluminating an incident point of excitation light and collecting fluorescent photons on the opposite side of the animal as the gantry was rotated 0, 45, 180, and 315 deg around the stationary animal. The fluorescent photon distributions were mapped onto the surfaces defined by CT as previously described.¹⁰

In order to perform GRFT, a linear, regularization-free reconstruction strategy was developed by neglecting the absorption coefficient of the fluorescence gene reporter at the excitation wavelength. In other words, the attenuation of excitation light from the gene reporter was assumed to be small compared to that from endogenous chromophores. With this assumption, the high-order SP₃ approximation achieves more accurate reconstruction quality when compared to the classic diffusion approximation (DA)¹¹ because a more precise solution to the forward problem of photon propagation is obtained from the

SP₃.¹²⁻¹⁴ Briefly, the linear, regularization-free reconstruction method needs to minimize the following least-squares problem:

$$\min_{0 < \mu_a^{\text{sf}} < \mu_a^{\text{sf,sup}}} \theta(\mu_a^{\text{sf}}) : \|A\mu_a^{\text{sf}} - J_T^{+,m,b}\|^2,$$

where $J_T^{+,m,b} = [J_1^{+,m,b}, \dots, J_{n_v}^{+,m,b}, \dots, J_{N_v}^{+,m,b}]^T$; $A = [G_1, \dots, G_{n_v}, \dots, G_{N_v}]^T$; T is a transpose operator; N_v is the number of fluorescent photon distribution from different illuminations at different positions; $J_{n_v}^{+,m,b}$ is the n_v -th measurable exiting partial current on the mouse surface; G_{n_v} denotes the relationship between the unknown absorption distribution μ_a^{sf} of the gene reporter and the n_v -th measurements $J_{n_v}^{+,m,b}$; and $\mu_a^{\text{sf,sup}}$ is the upper bound constraint of μ_a^{sf} . G_{n_v} was generated by using finite element methods and a series of matrix operations. More details can be found in Ref. 10. We used the limited memory variable metric-bound constrained quasi-Newton method¹⁵ to solve the least-squares problem for the linear, regularization-free GRFT. The algorithm was used to reconstruct the tumor-bearing, caudal regions of mice using tetrahedral volumetric meshing (Amira 5.0, Visualization Sciences Group, Burlington, MA). The meshes had an average element diameter of 1.0 mm and the number of the discretized points ranged from 17,000 to 22,000 depending on the CT volume of the selected regions. The absorption and scattering properties of the mouse were selected as 0.057 and 8.50 mm⁻¹ at both excitation and emission wavelengths, respectively.¹⁰ With the developed linear reconstruction algorithm, the reconstruction was performed on a cluster of eight nodes (eight CPU cores of 3.0 GHz and 16 GB RAM at each node) with the mapped fluorescent photon distribution.

For tumor imaging, the antibody-based agents were prepared by attaching a 1,4,7,10-tetraazacyclododecane-1,4,7,10-tetraacetic acid (DOTA) chelating agent to antibodies that target epithelial cell adhesion molecule using prior methods.¹⁶ A previously described flow cytometry method¹⁷ was used to assess the biological activity of the antibody conjugates and showed that conjugation of a DOTA chelating agent did not affect binding compared to unlabeled antibody. ⁶⁴Cu-labeling was performed with high radiochemical yields (>75%), and radiochemical purity was routinely >95% as determined by radio-thin-layer chromatography. The imaging agent was injected into the tail vein of tumor-bearing mice and trimodal imaging was performed 24 h after administration.

3 Results and Discussion

3.1 IFP1.4 Gene Reporter Fluorescence Tomography with *In Vivo* and *Ex Vivo* Validation

IFP1.4 mouse experiments were performed six weeks after orthotopic implantation of IFP1.4 transfected prostate tumor cells. Figure 1(a) to 1(d) illustrates the mapped IFP1.4 fluorescent photon distribution onto the mouse surface. Since the tumor locations varied from site of excitation and surface collection of fluorescence, distinct differences in fluorescent photon distribution occurred in the different views. The range of the ICCD exposure time was 600 to 1200 ms to maintain a similar photon count rate and five frames of data were averaged for each projection image to improve the signal-to-noise ratio. Figure 1(e) to 1(g) shows the *in vivo* trimodal tomographical results and *ex vivo* white and fluorescence images of the prostate tumor. As is

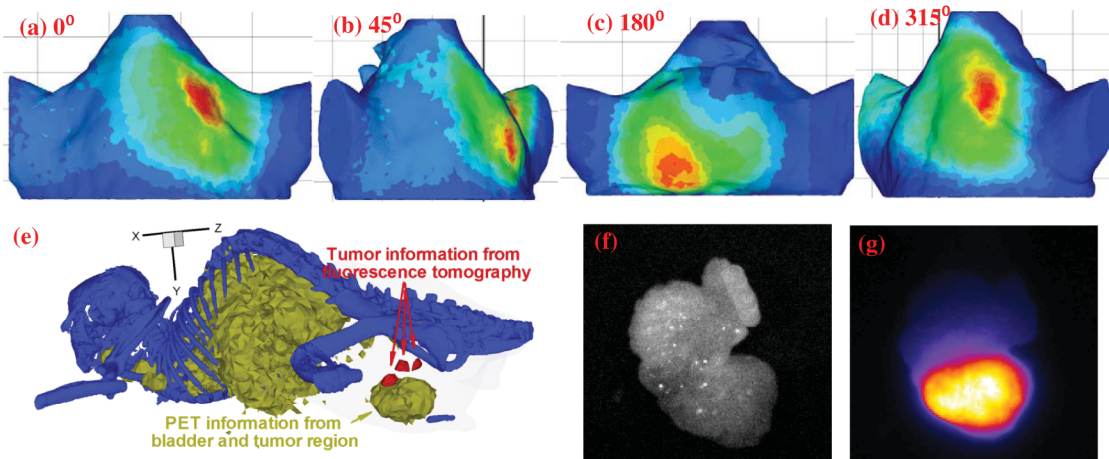


Fig. 1 IFP1.4 gene reporter fluorescence tomography six weeks after orthotopic cell injection with *in vivo* and *ex vivo* validation. (a) to (d) show the mapped fluorescent photon distribution on the mouse surface at four different views. (e) shows the trimodal (fluorescence/ μ PET/ μ CT) tomographic image results. Blue represents skeletal information from CT images; yellow represents PET imaging information; and red represents the reconstructed results of fluorescence tomography. The artifacts on the mouse surface are removed for better demonstration. (f) and (g) show the *ex vivo* white and fluorescent images of the prostate with tumor in *ex vivo* experiments.

typical with antibody imaging, clearance occurs through the liver; hence the PET signal can be seen within the abdomen, but GRFT imaging showed consistent location of tumors with PET signal in the prostate region. *Ex vivo* experiments show that the tumor has strong fluorescent signals. We found that PC3-IFP1.4 cells exhibited fast tumor growth compared to wild type (WT) or prior orthotopic studies employing PC3-DsRed.¹⁶ The

potential reason may be the effect of the virus transfection method and DNA combination. Although *in vivo* PET imaging can provide validation information, it is not always possible to discriminate bladder uptake from prostate uptake in the PET/CT images. Nonetheless, one can see that the fluorescence tomographic results in Fig. 1(e) are consistent with PET imaging of the tissue region containing the bladder and prostate. In

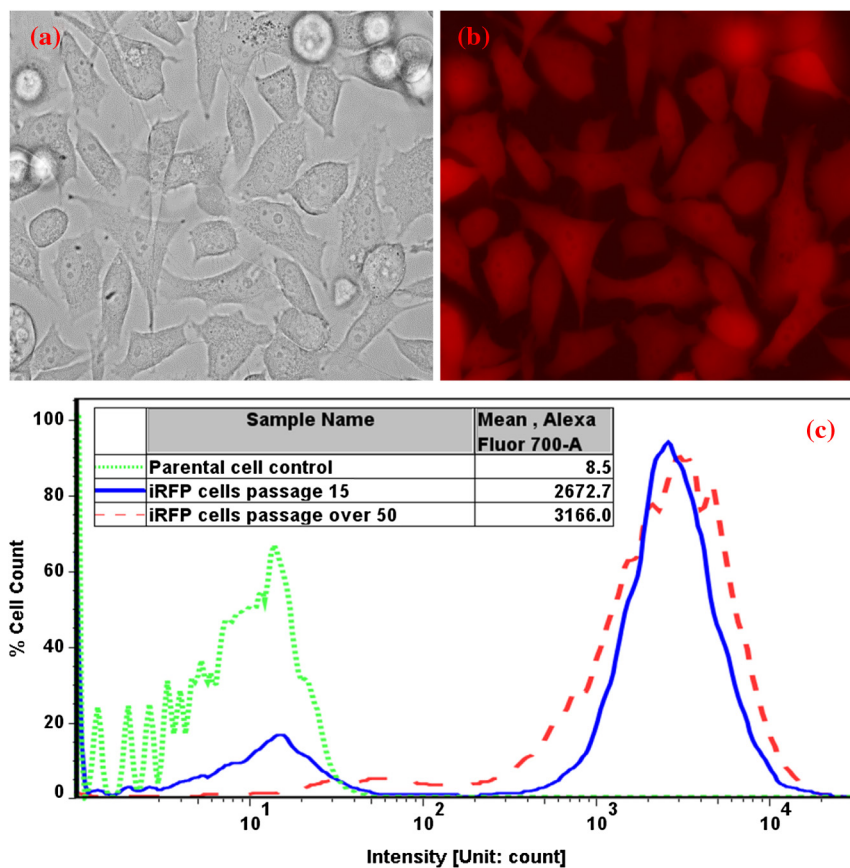


Fig. 2 PC3-iRFP cell imaging and stability analysis. (a) and (b) are the white and fluorescent images of the transfected PC3 cells. (c) is the stability analysis of the transfected PC3 cells by using flow cytometry. "Alexa Fluor 700-A" means that the fluorescent signals are collected by using Alexa Fluor 700-A filters. The table shows the mean channel intensity of each sample.

addition, *ex vivo* imaging confirms the IFP1.4 fluorescence arises from the prostate tumor [Fig. 1(f) and 1(g)].

3.2 *iRFP* Gene Reporter Fluorescence Tomography with *In Vivo* and *Ex Vivo* Validation

Because of the uncharacteristically rapid growth rate of PC3-IFP1.4 cells, we subsequently transfected cells with *iRFP*. Figure 2 shows the fluorescence imaging of the transfected cells. Fluorescence microscopy [Fig. 2(a) and 2(b)] confirms *iRFP* fluorescent protein expression. In order to analyze the stability of the cells, PC3-*iRFP* cells were carried in culture for several passages. Levels of *iRFP* expression were examined by flow cytometry using parental PC3 cells as a negative control. Figure 2(c) shows similar levels of *iRFP* expression in the transfectoma after 15 versus >50 passages in culture, compared to the parental PC3 cell line.

Five weeks after being orthotopically implanted with PC3-*iRFP* cells, mice were imaged as described above. The trimodal reconstruction results are shown in Fig. 3(a) with GRFT conducted with four projections. Figure 3(b) and 3(c) shows *ex vivo* white and fluorescent images of the prostate with tumor (~3.0 mm diameter) and strong fluorescent signals. When compared to an IFP1.4-based mouse model, although there is a one-week growth difference, the tumor size in an *iRFP*-based mouse model is smaller but similar to that previously reported by our group using PC3-DsRed. Although it is difficult to distinguish the bladder and prostate tumor regions from the PET and CT images, the reconstructed results in fluorescence tomography have similar size with the tumor and are close to the bladder and prostate tumor region in PET images [Fig. 3(a)].

3.3 Fluorescence Tomography for *iRFP* Gene Reporter at Different Tumor Stages

Imaging was performed at 4 ($N = 2$) and 10 to 12 weeks ($N = 2$) after orthotopic PC3-*iRFP* cell implantation. Figure 4(a) and 4(b) shows the trimodal reconstructed results for mice imaged 4 weeks and 10 weeks after implantation, respectively. When the tumor is at its early stage, the reconstructed

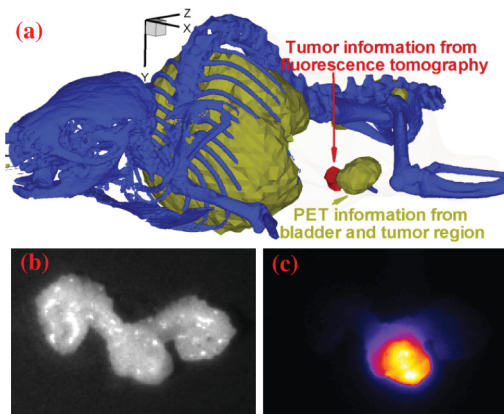


Fig. 3 *iRFP* gene reporter fluorescence tomography five weeks after orthotopic cell injection with *in vivo* and *ex vivo* validation. (a) shows the trimodal (fluorescence/ μ PET/ μ CT) tomographical results. Blue represents skeletal information from CT images; yellow represents the PET imaging information; and red represents the reconstructed results of fluorescence tomography. The artifacts on the mouse surface are removed for better demonstration. (b) and (c) show the white and fluorescent images of the prostate with tumor in *ex vivo* experiments.

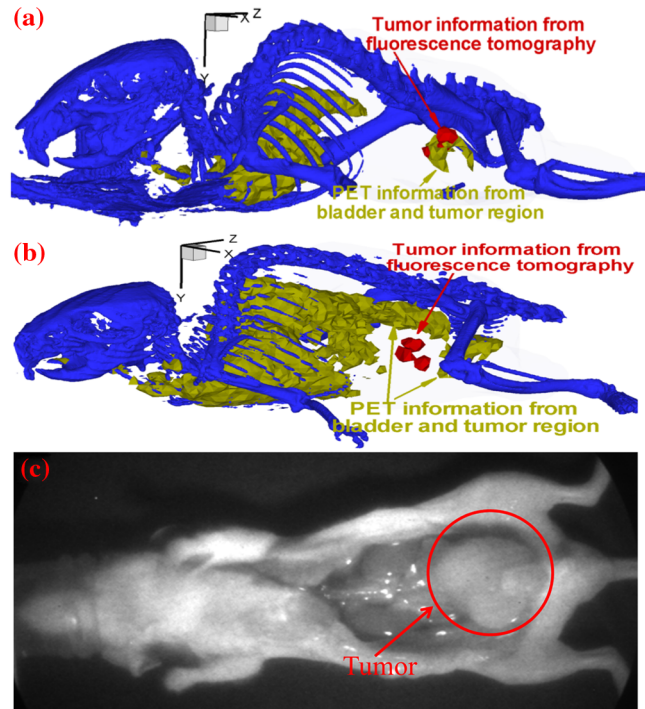


Fig. 4 *iRFP* gene reporter fluorescence tomography overlaid on CT and PET at different tumor stages. (a) and (b) are reconstructed results 4 and 10 weeks after cell implantation, respectively. Blue represents the skeletal information from CT images; yellow represents PET imaging information; and red represents the reconstructed results of fluorescence tomography. The artifacts on the mouse surface are removed for better demonstration. (c) *In situ* white light image for euthanized mouse depicted in (b) (the liver and intestine were removed).

results from fluorescence tomography agree well with PET imaging and are similar to the results shown in Fig. 3(a). However, later stage tumors were found after euthanasia to be massive (diameter ~30 mm) [Fig. 4(c)]. Although it is difficult to distinguish the bladder and tumor regions in Fig. 4(b), the *in vivo* PET images appeared to be restricted to the tumor boundary and excluded from the interior of the tumor due to the well-known restricted transport of macromolecules in solid tumors.¹⁸ In addition, the reconstructed *iRFP* source does not correspond to the size of the tumor for reasons which remain to be investigated. Nonetheless, *iRFP* signal originates from the center of the tumor region demarking the differences in localization expected between exogenously administered imaging agents and a gene reporter.

Table 1 Summary of fluorescent images in Fig. 5(a), 5(b), and 5(c).

Animal model	Intensifier gain	CCD integration times	Maximum photon counts
Tumor bearing			
Fig. 5(a)	7.4 V	1000 ms	44441.0
Fig. 5(b)	6.0 V	400 ms	52830.0
Nontumor-bearing control			
Fig. 5(c)	6.7 V	700 ms	7148.0

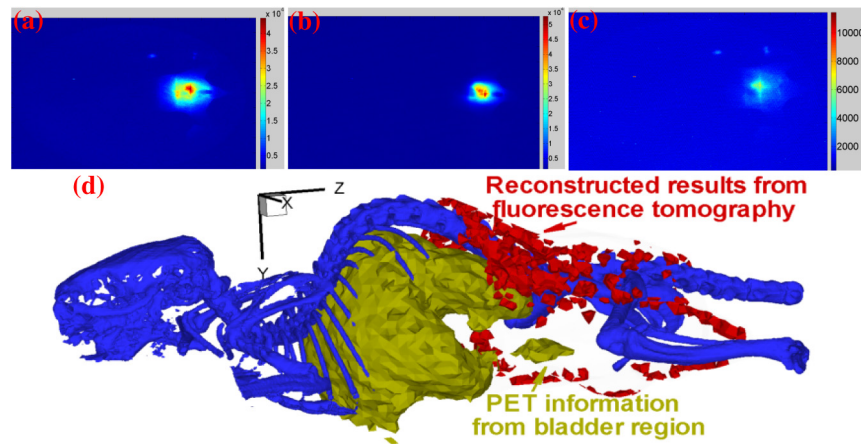


Fig. 5 Fluorescence imaging comparison between tumor- [(a) and (b)] and nontumor- (c) bearing mice and fluorescence tomography with nontumor-bearing mouse (d). The images were acquired from the ventral side of the mice. Blue represents skeletal information from CT images; yellow represents PET imaging information; and red regions are the reconstructed results of fluorescence tomography.

3.4 Gene Reporter Fluorescence Tomography with Control Mouse

In order to validate the stability of the developed GRFT and account for the effect of the excitation light leakage in the reconstructed results,^{11,19–21} a nontumor-bearing mouse was used as a control subject. Because the intensifier gain and exposure time of the imaging system affect the imaging counts, we set the intensifier gain and exposure time for the nontumor-bearing mouse to the averages of two tumor-bearing mice. The detailed settings and acquired maximal counts can be found in Table 1 and the acquired raw images from the ventral side of the mice are shown in Fig. 5(a) to 5(c). Although there is some excitation light leakage, the maximal counts in two tumor-bearing mice are higher than that in the nontumor-bearing mouse. The reconstructed results acquired with four-projections of surface fluorescent photon distributions are shown in Fig. 5(d). One can find that all the reconstructed values in fluorescence tomography appear artifactually on the mouse surface, which shows the robustness of the developed fluorescence tomography.

4 Discussion and Conclusion

Herein we demonstrated for the first time fluorescence tomography using far-red fluorescence gene reporters IFP1.4 and iRFP to image deep-seated orthotopic primary human prostate cancer in a mouse model. Due to the imprecise solutions with the classical DA, several high-order approximation models to the RTE have been developed to improve the reconstruction quality.⁵ Herein, we used the SP₃ high-order approximation due to its improved accuracy.¹⁴ Regularization methods are also popular for current implementation of nonlinear reconstruction strategies because of the ill-posed characteristics of fluorescence tomography. Although stable solution can be achieved from the regularization, the approach suffers from the need to select regularization parameters to achieve the appropriate image and therefore is susceptible to the “inverse” imaging crime.²² While the heterogeneous optical properties can affect time-independent measurements as made herein, anatomical information from CT or magnetic resonance imaging²³ and precise photon propagation models may further improve the reconstruction quality with *a priori* information. Although the image reconstructions conducted herein were performed with the assumption of a homogeneous optical property distribution, it is possible to

develop more complex reconstruction strategies using anatomical information.

Preliminary studies using IFP1.4 as a far-red gene reporter provided results similar to iRFP. However, the PC3-IFP1.4 cells exhibited more rapid tumor growth than PC3-iRFP or WT PC3 and resulted in centimeter-sized primary tumors, which may not be suitable for clinically relevant studies. Finally, the development of a near-infrared fluorescent gene reporter with excitation at wavelengths longer than 750 nm could further enhance fluorescence tomography by reducing the noise floor associated with autofluorescence that results from far-red excitation.

Acknowledgments

This work is supported in part by the National Institutes of Health Research Grant NIH R01 CA135673, a shared instrumentation grant to the Institute of Molecular Medicine Center for Flow Cytometry from the Cancer Prevention and Research Institute of Texas, the Texas Star Award (to E.M.S.), and a training fellowship from the Keck Center Computational Cancer Biology Training Program of the Gulf Coast Consortia (CPRIT grant number RP101489 to Y.L.).

References

1. C. H. Contag and M. H. Bachmann, “Advances in *in vivo* bioluminescence imaging of gene expression,” *Annu. Rev. Biomed. Eng.* **4**(1), 235–260 (2002).
2. K. E. Adams et al., “Comparison of visible and near-infrared wavelength-excitable fluorescent dyes for molecular imaging of cancer,” *J. Biomed. Opt.* **12**(2), 024017 (2007).
3. X. Shu et al., “Mammalian expression of infrared fluorescent proteins engineered from a bacterial phytochrome,” *Science* **324**(5928), 804–807 (2009).
4. G. S. Filonov et al., “Bright and stable near-infrared fluorescent protein for *in vivo* imaging,” *Nat. Biotechnol.* **29**(8), 757–761 (2011).
5. S. R. Arridge and J. C. Schotland, “Optical tomography: forward and inverse problems,” *Inverse Probl.* **25**(12), 123010 (2009).
6. M. Solomon et al., “Multimodal fluorescence-mediated tomography and SPECT/CT for small-animal imaging,” *J. Nucl. Med.* **54**(4), 639–646 (2013).
7. C. Li et al., “A three-dimensional multispectral fluorescence optical tomography imaging system for small animals based on a conical mirror design,” *Opt. Express* **17**(9), 7571–7585 (2009).

8. B. Zhu et al., "Non-invasive imaging of prostate cancer progression in nude mice using iRFP gene reporter," *Proc. SPIE* **8565**, 85651E (2013).
9. B. Zhu et al., "Tumor margin detection using quantitative, NIRF molecular imaging targeting EpCAM and validated by far-red gene reporter iRFP," *Mol. Imag. Biol.*, in press (2013).
10. C. D. Darné et al., "A compact frequency-domain photon migration system for integration into commercial hybrid small animal imaging scanners for fluorescence tomography," *Phys. Med. Biol.* **57**(24), 8135 (2012).
11. Y. Lu et al., "Improvement of fluorescence-enhanced optical tomography with improved optical filtering and accurate model-based reconstruction algorithms," *J. Biomed. Opt.* **16**(12), 126002 (2011).
12. A. D. Klose and E. W. Larsen, "Light transport in biological tissue based on the simplified spherical harmonics equations," *J. Comput. Phys.* **220**(1), 441–470 (2006).
13. M. Chu et al., "Light transport in biological tissue using three-dimensional frequency-domain simplified spherical harmonics equations," *Phys. Med. Biol.* **54**(8), 2493 (2009).
14. Y. Lu et al., "A parallel adaptive finite element simplified spherical harmonics approximation solver for frequency domain fluorescence molecular imaging," *Phys. Med. Biol.* **55**(16), 4625 (2010).
15. S. J. Benson and J. Moré, "A limited-memory variable-metric algorithm for bound-constrained minimization," Technical Report ANL/MCS-P909-0901, Mathematics and Computer Science Division, Argonne National Laboratory (2001).
16. M. A. Hall et al., "Comparison of mAbs targeting epithelial cell adhesion molecule for the detection of prostate cancer lymph node metastases with multimodal contrast agents: quantitative small-animal PET/CT and NIRF," *J. Nucl. Med.* **53**(9), 1427–1437 (2012).
17. M. A. Hall et al., "Quantifying multimodal contrast agent biological activity using near-infrared flow cytometry," *Contrast Media Mol. Imag.* **7**(3), 338–345 (2012).
18. R. K. Jain, "Physiological barriers to delivery of monoclonal antibodies and other macromolecules in tumors," *Cancer Res.* **50**(3 Suppl.), 814s–819s (1990).
19. K. Hwang et al., "Influence of excitation light rejection on forward model mismatch in optical tomography," *Phys. Med. Biol.* **51**(22), 5889 (2006).
20. E. M. Sevick-Muraca and J. C. Rasmussen, "Molecular imaging with optics: primer and case for near-infrared fluorescence techniques in personalized medicine," *J. Biomed. Opt.* **13**(4), 041303 (2008).
21. B. Zhu et al., "Reduction of excitation light leakage to improve near-infrared fluorescence imaging for tissue surface and deep tissue imaging," *Med. Phys.* **37**(11), 5961 (2010).
22. P. C. Hansen, *Discrete Inverse Problems: Insight and Algorithms*, Vol. 7, Society for Industrial and Applied Mathematics, Philadelphia, PA (2010).
23. A. Ale et al., "FMT-XCT: *in vivo* animal studies with hybrid fluorescence molecular tomography-X-ray computed tomography," *Nat. Methods* **9**(6), 615–620 (2012).